International Journal of Naval Architecture and Ocean Engineering 10 (2018) 393–402

Contents lists available at ScienceDirect

International Journal of Naval Architecture and Ocean Engineering

journal homepage: http://www.journals.elsevier.com/international-journal-of-naval-architecture-and-ocean-engineering/

A large scale simulation of floe-ice fractures and validation against full-scale scenario

Wenjun Lu [a, *], Hans-Martin Heyn [a, b], Raed Lubbad [a], Sveinung Løset [a]

[a] Sustainable Arctic Marine and Coastal Technology (SAMCoT), Centre for Research-based Innovation (CRI), Norwegian University of Science and Technology, Trondheim, Norway
[b] Centre for Autonomous Marine Operations and Systems (AMOS), Department of Marine Technology, Norwegian University of Science and Technology, Trondheim, Norway

ARTICLE INFO

Article history:
Available online 27 February 2018

Keywords:
Icebreaker
Ice
Splitting
XFEM
IMU

ABSTRACT

While interacting with a sloping structure, an ice floe may fracture in different patterns. For example, it can be local bending failure or global splitting failure depending on the contact properties, geometry and confinement of the ice floe. Modelling these different fracture patterns as a natural outcome of numerical simulations is rather challenging. This is mainly because the effects of crack propagation, crack branching, multi fracturing modes and eventual fragmentation within a solid material are still questions to be answered by the on-going research in the Computational Mechanic community. In order to simulate the fracturing of ice floes with arbitrary geometries and confinement; and also to simulate the fracturing events at such a large scale yet with sufficient efficiency, we propose a semi-analytical/empirical and semi-numerical approach; but with focus on the global splitting failure mode in this paper. The simulation method is validated against data we collected during the Oden Arctic Technology Research Cruise 2015 (OATRC2015). The data include: 1) camera images based on which we specify the exact geometry of ice floes before and after an impact and fracturing event; 2) IMU data based on which the global dynamic force encountered by the icebreaker is extracted for the impact event. It was found that this method presents reasonably accurate results and realistic fracturing patterns upon given ice floes.

1. Introduction

Fracturing of sea ice is one of the most visually significant events during ice-structure interactions. However, it is rather challenging to numerically simulate all the fracturing events which spans several scales, from local crushing, bending to the global splitting failure. Instead, we can focus on certain types of fractures and give corresponding appropriate treatment. For example, the local crushing has been treated with a plasticity model taking into account its energy dissipative nature without explicitly modelling the cracks (Liu et al., 2011). Modelling the bending failure is not so straightforward in a three-dimensional space. To the authors' knowledge, there exists not a complete set of numerical scheme to model the initiation and propagation of radial cracks; then the formation of circumferential cracks. These two types of cracks are usually studied separately, e.g., Nevel (1965), Lubbad and Løset (2011) proposed analytical solutions towards the radial crack initiation in a semi-infinite plate on a Winkler type foundation; and Lu et al. (2015b) studied the radial crack propagation within a finite square ice plate before circumferential crack's formation. In comparison, more studies were made on the eventual circumferential crack formation since it governs the final bending failure with a priori assumption of existing radial cracks, e.g (Nevel, 1958). In terms of the global splitting failure, it is less treated in literature and engineering practice. However, its importance in nowadays' Arctic marine operation should not be underestimated (Lu et al., 2015a, 2016). In this paper we adopted a numerical scheme based on which the global splitting failure can be modelled taking into account arbitrary geometries and contact scenarios. The basic numerical method is based on the eXtended Finite Element Method (XFEM), which alleviates us from constant re-meshing procedures to capture the near crack tip field variables (e.g., displacement). This allows us to model a stationary/propagating crack with improved

* Corresponding author.
E-mail address: wenjun.lu@ntnu.no (W. Lu).
Peer review under responsibility of Society of Naval Architects of Korea.

https://doi.org/10.1016/j.ijnaoe.2018.02.006

efficiency and accuracy. The numerical scheme is applied upon one interaction case and is compared against field measurement during the Oden Arctic Technology Research Cruise in the Arctic Ocean during September, 2015 (OATRC2015) (Lubbad et al., 2016). The effectiveness of the adopted numerically scheme to simulate the global splitting failure of an ice floe during ice-structure interaction is demonstrated in this paper.

2. Methods

In the field expedition of OATRC2015, icebreakers Oden and Frej were extensively instrumented with, e.g., camera systems to monitor the ice environment (ice thickness, ice concentration, and floe sizes), an Electro-Magnetic (EM) inductive device to continuously extract ice thickness, and Inertia Motion Units (IMUs) to get the global impact force during ice-structure interactions. These instrumentations provide necessary inputs for numerical setup and outputs for final comparison. Before we dive into the detailed methodology, it is convenient to first setup the floe-ice structure interaction model.

2.1. Interaction model

For floe ice–structure interactions, the assumed basic interaction model is described in Fig. 1. Side views in Fig. 1(a), (b) and (c) described the initial contact between ship hull and the gradually crushing at the ice edge, and eventually the hull-ice contact reached the full ice thickness. During this process, ice fractures at different scales are taking place. Rather small scale fractures are taking place at the crushed zone; relatively larger radial and circumferential cracks are formed due to the dominant vertical force from the sloping structure. Radial cracks are usually formed with relatively small vertical forces and they do not contribute to the final failure of an ice cover (Lu et al., 2015b). As the penetration proceeds to Fig. 1f), the ice cover can either fail continuously in local bending failure (i.e., formation of wedges and cusps) or in a global splitting failure (as depicted in the figure). Once the global splitting failure takes place, it is considered as the final limiting mechanism amongst all the fracture events.

Instead of simulating all these fracture events with one model from the very beginning, we decide to treat them separately with correspondingly appropriate models. For example, the local crushing has been effectively described by plasticity theories (Liu et al., 2011); by an energy based contact model (Daley, 1999); or the specific energy in a crushed volume approach (Kim and Høyland, 2014; Kinnunen et al., 2016). The local bending failure can be treated either with theoretical formulas (Nevel, 1958, 1972) or empirical formulas (Kerr, 1976) (originally from (Panfilov, 1960)). Combining all these approaches, we are thus analysing the floe ice–structure interaction in a semi-analytical/empirical and semi-numerical manner. This paper, however, focuses primarily on the global splitting failure's numerical simulation.

In order to simulate the splitting failure of an ice floe, it is necessary to gain information such as the floe geometry, ice thickness and impact angle as inputs. Afterwards, a numerical scheme based on eXtended Finite Element Method (XFEM) is initiated and output the splitting force history versus splitting crack propagation. In the end, the calculated splitting force is compared with measurements from IMUs. In later sections, the method adopted within each of these steps is described. Particularly, we shall focus on the instrumentations and interaction scenarios on the icebreaker Frej.

2.2. Ice floe geometry extraction

The geometry of an ice floe is extracted from images taken by an 180° camera system that has four lens looking in different directions covering the majority of the area on the port and starboard sides of Frej. Detailed camera system information, installation location and calibration methods onboard Frej can be found in Lu

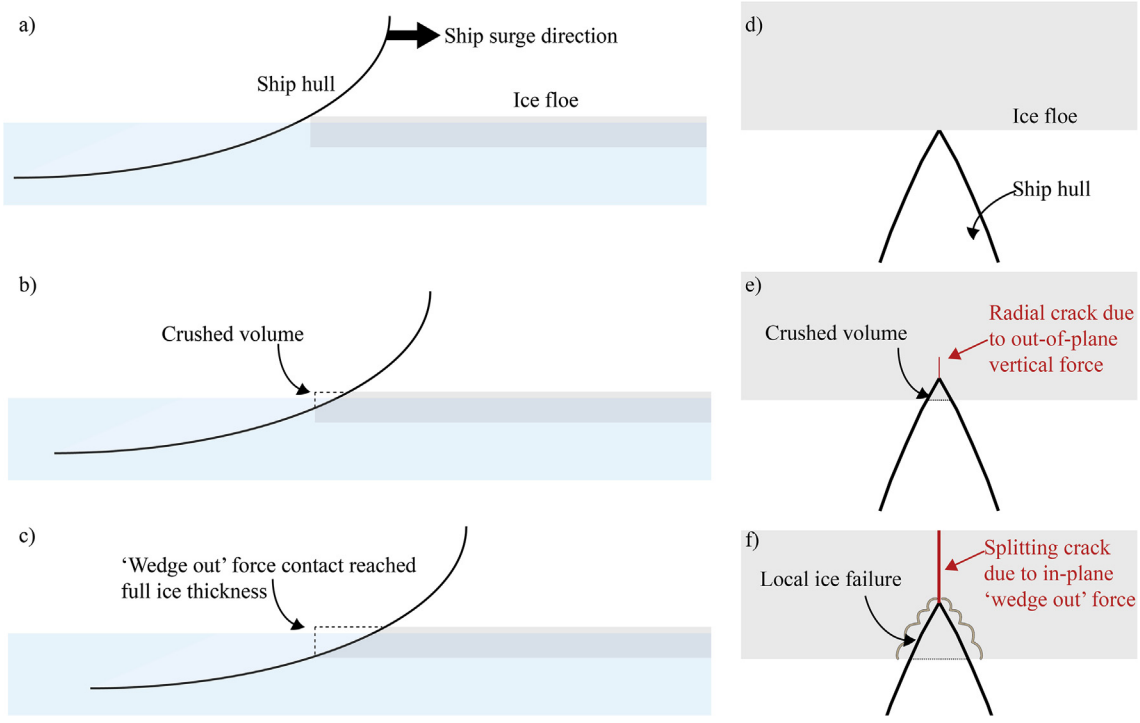

Fig. 1. Floe ice–structure interaction model (left: side view; right: plan view).

et al. (2016a; 2016b).

In general, chessboards with known geometry were placed within the viewing field of the camera lens to be calibrated (see Fig. 2 a and b); afterwards, the method developed by Geetha and Murali (2013) was adopted to rectify 'Fig. 2 a and b' into 'c and d', respectively. After perspective rectification, the ice floe's geometry and size information are available.

In terms of ice thickness, both the EM device and another camera system are available to continuously monitoring the interested ice floe's thickness (Lu et al., 2016b).

2.3. Simulating the splitting crack with XFEM

Given an ice floe of arbitrary geometry, the splitting crack propagates in a rather nonlinear fashion. In order to capture the crack propagation path correctly, usually a rather refined mesh at the crack tip is required to gain sufficient stress field information and thereby to determine the crack propagation direction (Anderson, 2005). Therefore accordingly, as the crack propagates, continuous mesh refinement at the crack tip would be required. Ingraffea and Wawrzynek (2004) made extensive reviews on different methods to simulate fractures. Aside from the approach that requires extensive computational power to update the mesh geometry as crack propagates, one can also resolve to use mesh free or meshless methods. The XFEM is one of such methods that minimal mesh refinement is needed to capture arbitrary crack path and crack tip singularity because of the additionally enriched degree of freedoms (Belytschko and Black, 1999). Eq. (1) illustrates the basic formulation of the XFEM, in which, the first term on the Right Hand Side (RHS) represents the conventional FEM with nodal displacement of $\mathbf{u}_i$ multiplying the shape function $N_i(x)$; the second term on the RHS applies to the nodes $\mathbf{a}_i$ of enriched elements that are cut through by the crack and describes the displacement jump over a crack by additionally multiplying the Heaviside function $H(x)$; and the third term applies to the element which encompasses the crack tip describing the near tip displacement by additionally multiplying the function $F_\alpha(r,\theta)$, which is expressed in Eq. (2) with polar coordinate r and θ with origin at the crack tip (see Fig. 3). Both $\mathbf{a}_i$ and $\mathbf{b}_i^\alpha$ are nodal enriched degree of freedom vectors.

$$\mathbf{u} = \sum_{i=1}^{n} N_i(x)\left[\mathbf{u}_i + H(x)\mathbf{a}_i + \sum_{\alpha=1}^{4} F_\alpha(r,\theta)\mathbf{b}_i^\alpha\right] \tag{1}$$

$$F_\alpha(r,\theta) = \left[\sqrt{r}sin(\theta/2) \quad \sqrt{r}\cos(\theta/2) \quad \sqrt{r}sin(\theta)sin(\theta/2) \quad \sqrt{r}sin(\theta)cos(\theta/2)\right] \tag{2}$$

This paper employs the XFEM functionality within ABAQUS to evaluate the Stress Intensity Factors (SIFs) so as to determine the crack's propagation. With known SIFs $K_I(a)$ and $K_{II}(a)$ at given crack length a, the crack propagation direction can be identified either based on the maximum energy release rate direction; or the $K_{II}(a+\Delta a) = 0$ criteria. For most engineering application purposes, both methods give similar results (Hutchinson and Suo, 1991). This is also confirmed by an earlier study on parallel channel crack propagation in ice (Lu et al., 2015c). In this paper, we adopt the

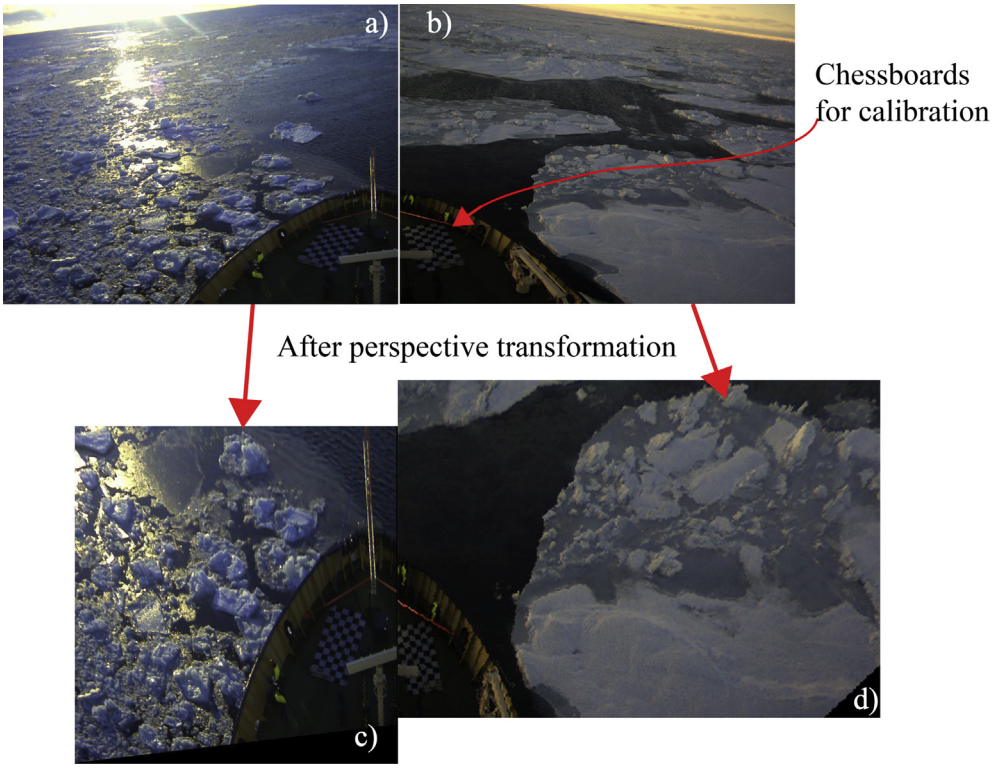

Fig. 2. Calibration and perspective rectification of the ice condition images.

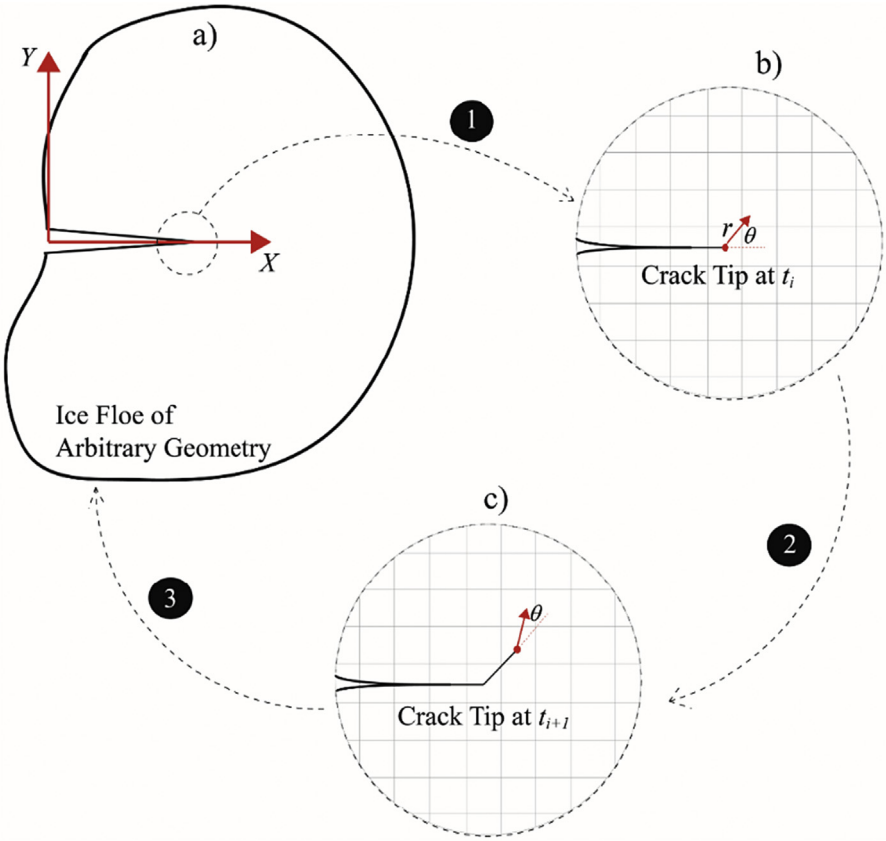

Fig. 3. Crack propagation direction and model update.

$K_{II}(a+\Delta a)=0$ criteria to identify the propagating direction θ of the crack by solving Eqs. (3) and (4).

$$K_{II}(a+\Delta a)=C_{21}K_I(a)+C_{22}K_{II}(a) \tag{3}$$

$$\begin{aligned} C_{21} &= 1/4[sin(\theta/2)+\sin(3\theta/2)] \\ C_{22} &= 1/4\cos(\theta/2)+3/4cos(3\theta/2) \end{aligned} \tag{4}$$

The general flowchart of the calculation is illustrated in Fig. 3. The whole procedure in Fig. 3 is automated to simulate the crack propagation within an ice floe of arbitrary geometry. For each crack configuration, the same mesh is used so as to minimize computational efforts in remeshing thanks to the elegance of XFEM. The only geometry that needs to be updated during each consecutive simulation is the crack configuration. Specifically, Steps #2 and #3 described in Fig. 3 is implemented within Matlab to generate a pre-processing Python script containing updated crack information to feed to ABAQUS. The calculated results are further extracted by another post-processing Python script to feed to Matlab updating the crack geometry for a new loop of simulation. Following the coordinate system defined, the splitting force $F_{splitting}(X=0)$ versus crack extension a can be correlated with the calculated SIFs as in Eq. (5).

$$\begin{aligned} K_{total}(a) &= \sqrt{K_I^2(a)+K_{II}^2(a)} \\ F_{splitting}(X=0,a) &= \frac{K_{IC}}{K_{total}(a)} \end{aligned} \tag{5}$$

In which,

$K_I(a)$ and $K_{II}(a)$ are the Mode I and II SIFs at the crack tip with crack length a under a unit loading at the crack mouth $X=0$;
$K_{total}(a)$ is the combined SIF effect;
K_{IC} is the fracture toughness of sea ice;
$F_{splitting}(X=0)$ is the splitting force acting at $X=0$ pointing towards the positive and negative Y directions.

The above described numerical scheme enables us to capture the splitting force versus crack propagation path, both of which are simulation results by themselves. Comparing to other classic computational fracture mechanics approaches (Ingraffea and Wawrzynek, 2004), we do not need information about the actual crack path in advance.

2.4. Back calculation of impact force from IMUs

In order to compare with the calculated results, the IMUs' measurement are utilized. The icebreaker Frej was equipped with four IMUs of type ADIS 16364 and ADIS 16480. IMU 1 was placed directly underneath the bridge level, IMU 2 midship in a compartment in the bow of the vessel; IMU 3 was placed directly on the hull in the bow of the vessel at the port side and IMU 4 on the hull of the vessel on the opposite side (starboard). During the expedition, IMU 2 experienced a malfunction and had to be discarded. IMU 1 was the only ADIS 16480 type sensor and the difference to the other sensor was, that IMU 1 was capable to output the ship's altitude, which is not required for this work. The placement of the sensors is illustrated in Fig. 4.

Besides the altitude from IMU 1, all IMUs measured the acting acceleration on them in all linear directions and the angular rates in all three directions. For this work, we consider only the acceleration

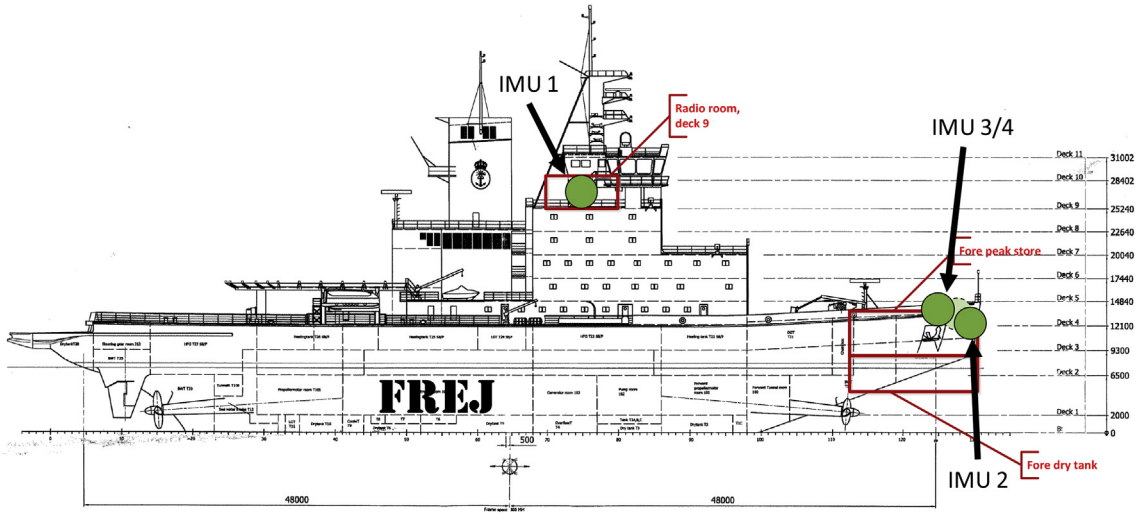

Fig. 4. Placement of IMUs on the icebreaker Frej.

Table 1
Parameters of the icebreaker Frej

m_{ship} [kg]	780×10^4
m_{add} [% of m_{ship}]	10, 20 and 30
d_{11} [kg·s^{-1}]	2.141×10^4

Table 2
Biases of the accelerometer in IMU 1.

$b_{1,x}$ [mg]	−5.79
$b_{1,y}$ [mg]	6.77
$b_{1,z}$ [mg]	12.60

output of each sensor, which is given in Eq. (6).

$$\boldsymbol{a}^s_{m,i} = \mathbf{R}^b_s(\psi_i)^{\mathrm{T}}\left(\dot{\mathbf{v}}^{\boldsymbol{b}} - \mathbf{g}^{\boldsymbol{b}}\right) + \mathbf{b}^s_{\boldsymbol{i}} + \boldsymbol{\omega}^s_{\boldsymbol{i}} \tag{6}$$

$\mathbf{R}^b_s(\psi_i)\in\mathbb{R}^{3x3}$ is a rotation matrix to correct for the difference between the sensor's inertial frame and the body-fixed reference frame of the vessel, $\dot{\mathbf{v}}^{\boldsymbol{b}}\in\mathbb{R}^3$ is the acceleration acting on the sensor, $\mathbf{g}^b = \mathrm{col}(0,0,g)$ contains the earth's gravity, $\boldsymbol{b}^s_i\in\mathbb{R}^3$ are the accelerometer's biases and $\boldsymbol{\omega}^s_i\in\mathbb{R}^3$ accounts for measurements noise. For the measurements, we selected days with as little wind as possible to allow for the negligence of wind induced accelerations. Because the ship was travelling in ice, the influence of waves has been neglected as well. The acting acceleration contains under these assumptions

$$\dot{\mathbf{v}}^b = \mathbf{a}^b_{hyd} + \mathbf{a}^b_{prop} + \mathbf{a}^b_{ice} \tag{7}$$

with $\mathbf{a}^b_{hyd}\in\mathbb{R}^3$ containing the accelerations caused by hydrodynamic and hydrostatic forces, $\mathbf{a}^b_{prop}\in\mathbb{R}^3$ the propeller induced accelerations and $\mathbf{a}^b_{ice}\in\mathbb{R}^3$ the ice induced accelerations.

Assuming further a constant speed and heading of the vessel before impact with the ice feature and taking only the surge acceleration of the vessel into account, we can assume that the hydrodynamic forces are compensated by the propeller thruster. This means that the measured acceleration upon impact with the ice feature contains the ice induced acceleration as its dominant component

$$\mathrm{a}^b_{ice,surge} = \mathbf{B}_{\mathbf{x}}\mathbf{R}^b_s(\psi_i)\left(\mathbf{a}^s_{m,i} - \mathbf{b}^s_{\boldsymbol{i}} - \boldsymbol{\omega}^s_{\boldsymbol{i}}\right) \tag{8}$$

where $\mathbf{B}_{\mathbf{x}} = (1,0,0)$ is a selection matrix to pick only the surge acceleration. The bias of each sensor is removed by a calibration procedure and the noise of each sensors is filtered out in post processing by a Butterworth low pass filter. The bias of each accelerometer was determined on land before the expedition under laboratory conditions by comparing the gravity measurements of

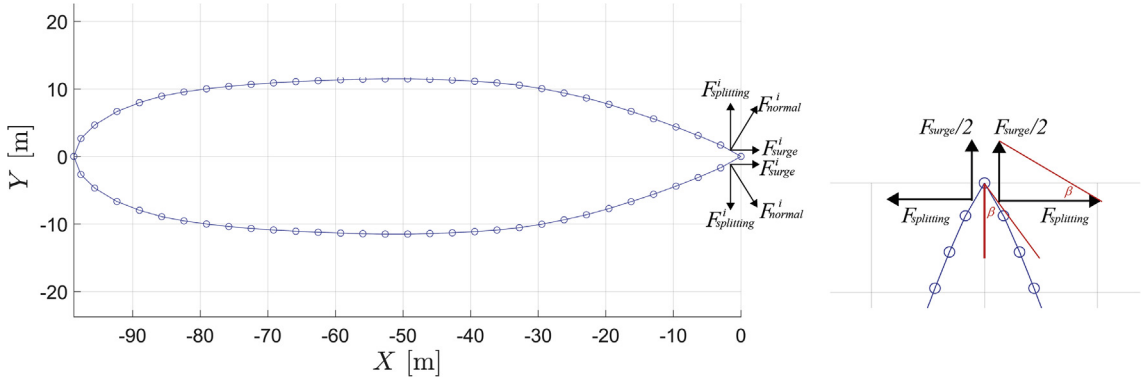

Fig. 5. Waterline geometry of Frej and the assumed contact force decomposition.

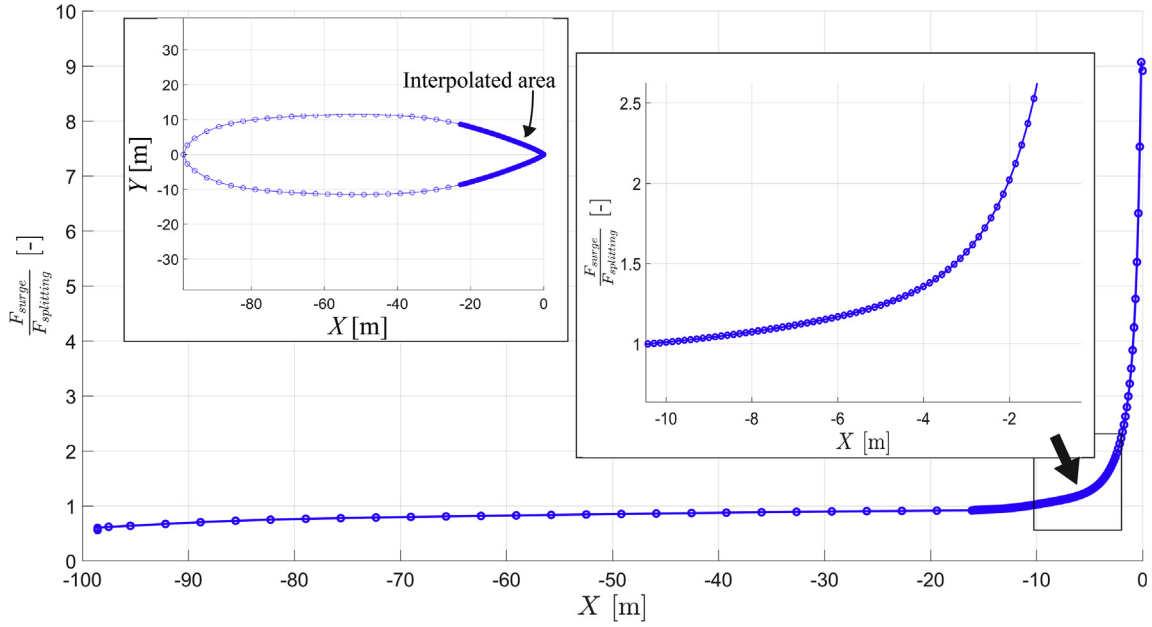

Fig. 6. Ratio between the impact force in the surge direction and splitting force based on the waterline geometry of Frej.

each sensor with the results from a calibrated reference sensor (xIMU from x-io technologies). The results from the calibration are shown in Table 2. Bjerkås et al. (2007) and Kjerstad et al. (2015) found that the global ice load signal only contains frequency components up to a maximum of 5 Hz. Therefore the cut-off frequency for the low-pass filter was set to 5 Hz to ensure that only ice induced accelerations are recorded.

The force in surge direction can be evaluated by knowing the total acting mass $m_{11} = m_{ship} + m_{add}$, which contains the ship's displacement mass and the added mass due to the surrounding water masses. Furthermore, an additional damping, with the damping parameter d_{11}, due to the contact of the lower ship hull with water can be assumed. The measured ice induced acceleration then contains

$$a^b_{ice,surge} = m_{11}^{-1} \cdot F_{surge} + d_{11}^{-1} \cdot u_{surge} \tag{9}$$

The velocity in surge direction of the vessel is u_{surge} and the ice induced surge force is F_{surge}. In case the hydrodynamic damping is neglected, the second term of the equation is zero. The force in surge direction is then given as

$$F_{surge} = m_{11} \cdot a^b_{ice,surge} \tag{10}$$

The parameters of the icebreaker Frej are given in Table 1.

2.5. Relationship between splitting force and impact force

The previous two sections introduced calculation methods of splitting force and impact force separately. However, these two force are not directly comparable. A certain relationship concerning

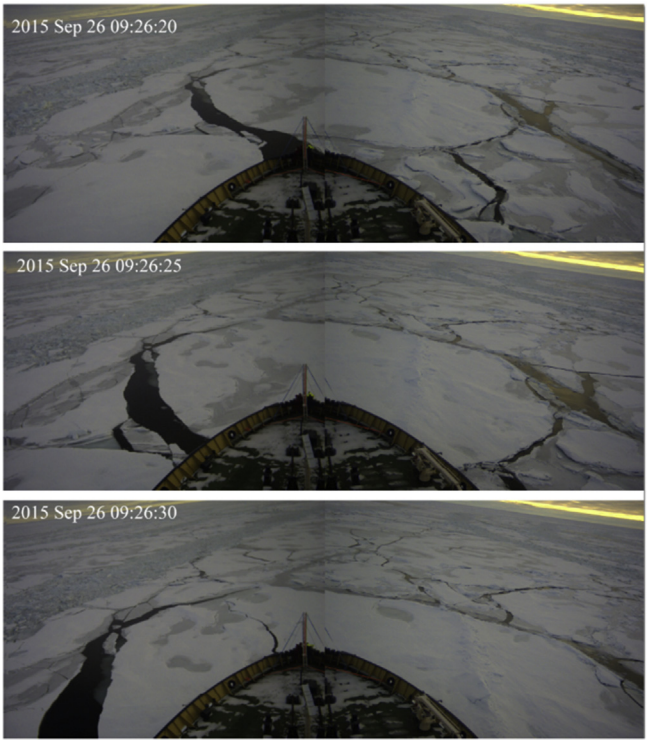

Fig. 7. An ice floe's splitting failure scenario chosen for case study.

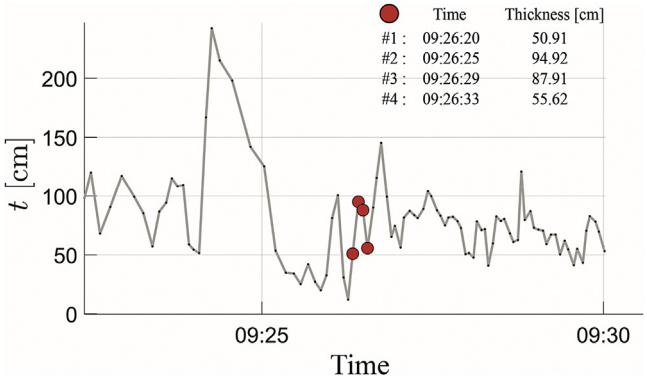

Fig. 8. Ice thickness history measured by the on board Electro-Magnetic inductive device.

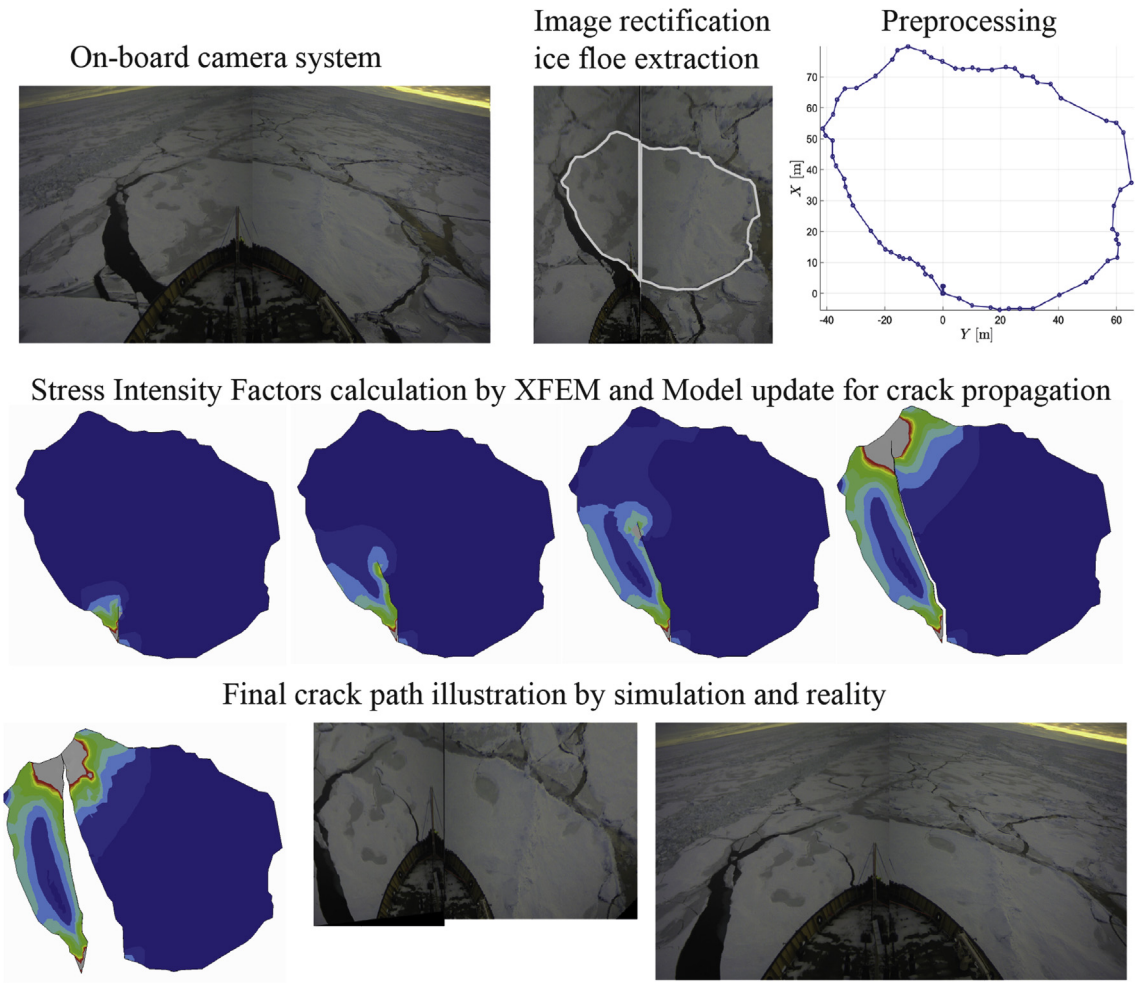

Fig. 9. Crack path within the selected ice floe before and after the fracture in both the simulation and reality.

the contact properties has to be constructed to correlate these two terms. This paper assumed a perfectly full contact between the structure and ice floe. During the initial ice-structure interaction before global splitting failure occurs, the stress field within the overlapped area between structure and ice floe is assumed to be averaged upon each hull panel. Based on this assumption, the contact force decomposition between the structure and ice floe reduces to a geometrical problem and the impact force in the structure's surge direction F_{surge} can be correlated to the splitting force $F_{splitting}$ solely based on the structural geometries. Take the icebreaker Frej as an example, the waterline geometry is plotted in Fig. 5 together with contact force decomposition in the splitting and surge direction, respectively. The waterline plot is composed of a series of panels with area A^i, angle β_i (see the definition of angle β in Fig. 5) for each panel i ; and F_{surge} and $F_{splitting}$ can be correlated as in Eq. (11) if we consider only half part (e.g., $Y \geq 0$ on the port side) of the symmetric ship.

$$\frac{F_{surge}}{F_{splitting}} = \frac{2\sum_{i=1}^{N} F^i_{surge}}{\sum_{i=1}^{N} F^i_{splitting}} = \frac{2\sum_{i=1}^{N} A^i \sin\beta_i}{\sum_{i=1}^{N} A^i \cos\beta_i} \tag{11}$$

Given the geometric properties of Frej, the ratio between surge and splitting forces, i.e. Eq. (11), is shown in Fig. 6 as a function of the penetration. Here we assume that the splitting occurs while the 'wedge out' force reached the full ice thickness as in Fig. 1(c). One can see from Fig. 6 that as the penetration increases, the ratio between the impact force and splitting force decrease gradually as an increasing component in the splitting direction (i.e., Y direction) appears. In the following case study, the ice floe thickness is about 1.0 m based on field measurements. Considering the sloping angle of Frej, the scenario Fig. 1(c) corresponds to a penetration of 2.5 m. A zoomed in sub-figure in Fig. 6 illustrates that the ratio

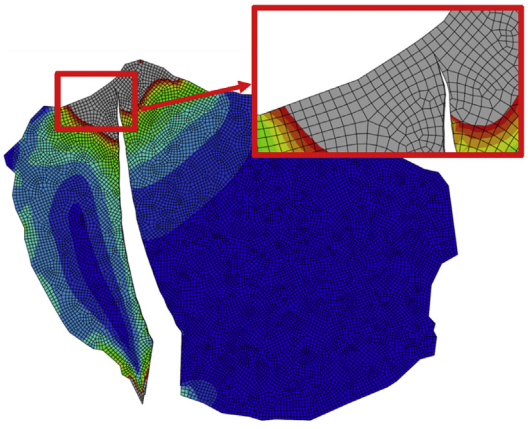

Fig. 10. Illustration of crack path's mesh independency.

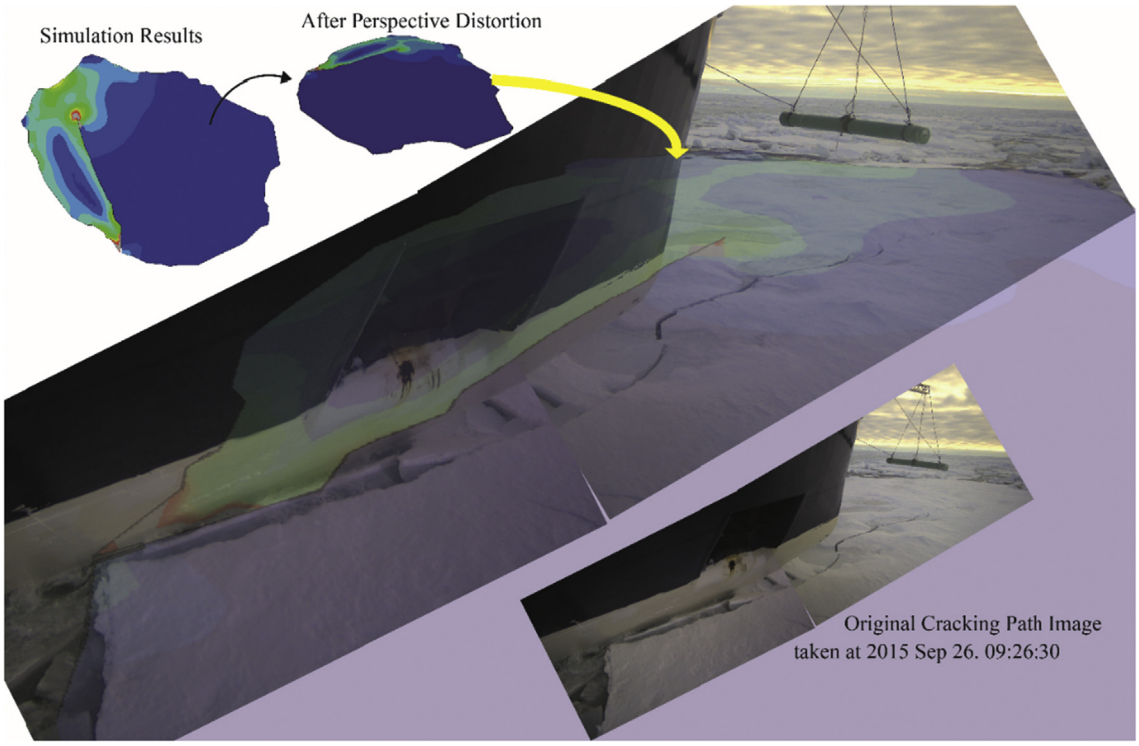

Fig. 11. Overlay of the simulation results with actual crack path image.

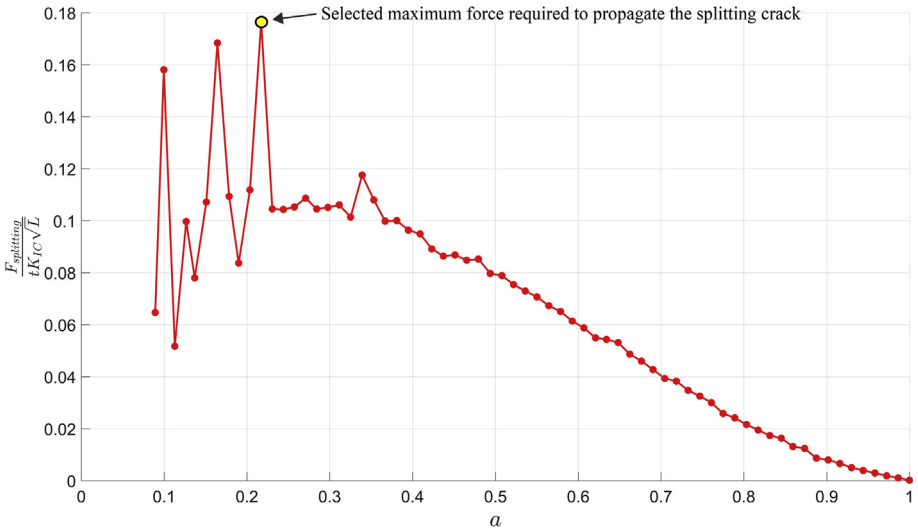

Fig. 12. Normalized splitting force versus normalized crack distance by simulation.

$F_{surge}/F_{splitting}$ is around 1.8. This value shall be used for later comparison.

3. Case studies

With the above described numerical scheme, a case study is carried out in this paper. The selected case is a splitting scenario of an ice floe while interacting with the icebreaker Frej. It took place from 09:26:20 to 09:26:30 (UTC time) on September 26th, 2015 in the Arctic Ocean. The selected case with the interaction process is shown in Fig. 7: after an eccentric impact, a splitting crack eventually took place within the ice floe and kinked sideways. During this period, the measured ice thickness history is presented in Fig. 8.

Based on the perspective rectification process described earlier, the captured images in Fig. 7 were utilized to extract the ice floe's pre-failure geometries shown in the 1st row of Fig. 9. Then the geometric information together with the loading point (i.e., at $X = 0$ and $Y = 0$) is provided by Matlab and passed over to ABAQUS (via the generated preprocessing Python script) calculating the SIFs at different crack configurations.

Within each of the consecutive simulations, the crack geometry is updated according to the solution from Eqs. (3) and (4). The 2nd row of images in Fig. 9 shows the stress field and also the

Table 3
Inputs for the calculation of splitting force.

$\max(F_{splitting}/(tK_{IC}\sqrt{L}))$	0.1766
t [m]	1 (ref.: Fig. 8)
L [m]	75
K_{IC_lower} [kPa$\sqrt{\text{m}}$]	115
K_{IC_upper} [kPa$\sqrt{\text{m}}$]	250
$F_{surge}/F_{splitting}$	1.8

Table 4
Impact force in the surge direction calculated based on the ice splitting failure simulations.

$F_{splitting\_lower}$[kN]	$F_{splitting\_upper}$ [kN]	F_{surge_lower}[kN]	F_{surge_upper} [kN]
161.81	351.76	291.26	633.17

propagating crack. At the crack tip, stress concentration is also shown. The eventual failure of the ice floe is shown in the 3rd row of Fig. 9 for both the simulation results and field observations. In addition, the major merit of XFEM, i.e., crack paths' mesh independency, is illustrated in Fig. 10. The solution-dependent crack cuts through the pre-defined mesh pattern.

4. Results and discussions

Crack propagation track shown in the 2nd row of Fig. 9 visually agrees well with the reality, but not exactly. In both cases, the crack propagates to the upper-left corner of the ice floe. However, the crack path is not identical. Exact matching the simulated crack path with the field observation is rather challenging for the current case study. During the OATRC2015 expedition, there was one camera installed at the bow area on the starboard side of Frej. The fracture event at the exact time of the chosen case is also captured by the bow camera. Fig. 11 qualitatively compares the crack path by intuitively overlaying two images together. Fig. 11 shows that the simulation results do not coincide exactly with the actual crack, however, the general crack propagation direction is the same. The discrepancy is considered to be caused by: 1) an 'imperfect' contact exists between the structure and the ice floe; 2) inhomogeneity within the ice floe. In the simulation, a full contact between ice and the structure is assumed. This assumption is different from what Fig. 11 shows, in which, local failures create non-smooth ice-structure contact. These additional local fractures lead to an imperfect contact as compared with the numerical simulation input, thereby creating a relatively different boundary condition. One can also see from Fig. 11 that the crack kinks into a melt pond which is believed to be a weak zone within the ice floe. However, in the simulation, the ice floe is assumed to be a homogeneous plate.

The splitting force $F_{splitting}(X=0)$ is normalized by dividing $(tK_{IC}\sqrt{L})$, in which, t is the ice thickness and L is the floe size in the surge direction. Fig. 12 illustrates the normalized splitting force $F_{splitting}/(tK_{IC}\sqrt{L})$ versus the normalized crack length a (i.e., crack location divided by the total crack length). The results show that the maximum splitting force required to propagate the splitting crack through the entire ice floe occurs at about 22% of the final crack length.

Next, the simulated splitting force $F_{splitting}(X=0)$ is converted into the impact force in the surge direction F_{surge} based on hull geometric considerations of Frej (see Fig. 5) and further compared with measurement from IMUs. The comparison together with selected material parameters and other coefficients are shown in Tables 3 and 4. Since we did not measure the fracture toughness of sea ice, we choose two existing values in literature (Dempsey et al., 1999; Schulson and Duval, 2009) representing the lower and upper values, respectively. The final impact force in the surge direction based on ice failure simulation are presented in Table 4 with both the lower and upper values.

In the current selected case study, there were three working IMUs. However, a great scatter of impact force were back calculated by the IMUs' measurements. Notably, IMUs 3&4 predicted much larger impact force (around one magnitude larger) than the simulation results in Table 4. On the other hand, back calculated impact force in the surge direction from IMU 1 agrees well with the predicted force in Table 4. This is illustrated in Fig. 13. Considering the fact that IMU 1 is installed on the bridge, lots of local vibrations have been damped out such that the global acceleration of the ship during the interaction can be reasonably well extracted. As for IMUs 3 and 4, they were installed near the bow area, which is susceptible to local hull vibrations during the interaction. This may cause too much impact force based on the presented back calculation method. Aside from the IMUs' measurements, strain gauges were also installed at the ship bow area. It would be beneficial to include the strain gauges' measurement for a more complete comparison. On the other hand, correlating F_{surge} and $F_{splitting}$ by Eq. (11) might be oversimplified, especially considering there is a dramatic change on $F_{surge}/F_{splitting}$ at the initial penetration as illustrated by Fig. 6. This is speculated to be the reason of the slight overshooting of the IMU 1 based measurement over the simulation based prediction F_{surge_upper} in Fig. 13.

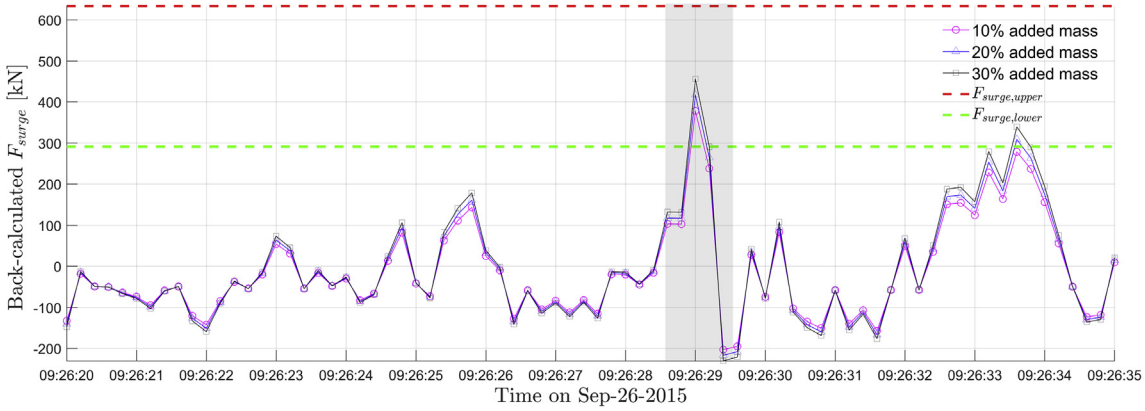

Fig. 13. Comparison of F_{surge} obtained by ice floe fracture simulation and IMU 1's back calculation based on $f_{cutoff} = 5$ Hz.

5. Conclusions

This paper presents a novel approach to simulate the fracture of an ice floe during ice–structure interactions. The key idea is that different fractures at different scales are treated differently. We focused on the splitting failure mode and proposed a numerical scheme based on the eXtended Finite Element Method to simulate a splitting crack's propagation. Given the contact properties, and floe geometries, the nonlinear splitting crack propagation path can be numerically predicted together with the required splitting force history. The numerical scheme is applied in one case study with one interaction scenario during the Oden Arctic Technology Research Cruise in September of 2015. During the research cruise, field measurements such as floe geometry and ice thickness were extracted by a camera system and an Electro-Magnetic inductive device, respectively. In addition, the global interaction force can be back calculated by the installed Inertia Motion Units (IMUs). With the measured floe geometry and ice thickness, the developed numerical scheme predicts the crack path rather effectively. The general trend and propagation direction of the crack in the simulations agree rather well with reality, although an exact path prediction were not achieved, possibly due to inhomogeneity in ice and imperfect contact between ice and structure as assumed in the numerical scheme. In addition to the favorable visual agreement on crack paths, the simulated impact force based on the floe ice's splitting failure was compared with back calculated results from IMUs' measurements. It turned out that not all IMUs give the same impact force, possibly due to local hull vibrations. However, one of the IMUs, which was installed at the bridge, measured an impact force; and the value is well within the range of the numerical simulations. The current mutual agreement between simulated results and field measurement is encouraging. This paper demonstrates the potential of the proposed method and recommends for the method's further development and validations.

Acknowledgements

The authors would like to thank the Research Council of Norway through the research center SAMCoT CRI for financial support and all the SAMCoT partners. In addition, Oden Arctic Technology Research Cruise 2015 (OATRC2015) was supported by the ExxonMobil Upstream Research Company and performed by the Norwegian University of Science and Technology (NTNU) in cooperation with the Swedish Polar Research Secretariat (SPRS) and the Swedish Maritime Administration (SMA).

References

Anderson, T.L., 2005. Fracture Mechanics: Fundamentals and Applications. CRC press.

Belytschko, T., Black, T., 1999. Elastic crack growth in finite elements with minimal remeshing. Int. J. Numer. Meth. Eng. 45 (5), 601–620.

Bjerkås, M., Skiple, A., Iver Røe, O., 2007. Applications of continuous wavelet transforms on ice load signals. Eng. Struct. 29 (7), 1450–1456.

Daley, C., 1999. Energy Based Ice Collision Forces. In: Proceedings of the 15th International Conference on Port and Ocean Engineering under Arctic Conditions. Helsinki University of Technology in Espoo, Finland.

Dempsey, J.P., Adamson, R.M., Mulmule, S.V., 1999. Scale effects on the in-situ tensile strength and fracture of ice. Part II: first-year sea ice at Resolute, NWT. Int. J. Fract. 95 (1), 347–366.

Geetha, A., Murali, S., 2013. Automatic rectification of perspective distortion from a single image using plane homography. IJCSA 3 (5), 47–58.

Hutchinson, J.W., Suo, Z., 1991. Mixed mode cracking in layered materials. Adv. Appl. Mech. 29, 63–191.

Ingraffea, A.R., Wawrzynek, P.A., 2004. Computational fracture mechanics a survey of the field. In: European Congress on Computational Methods in Applied Science and Engineering.

Kerr, A.D., 1976. The bearing capacity of floating ice plates subjected to static or quasi-static loads. J. Glaciol. 17, 229–268.

Kim, E., Høyland, K., 2014. Experimental investigations of the energy absorption capacity of ice during crushing: is the specific energy scale independent?. In: Proceedings of the 22nd IAHR International Symposium on Ice, Singapore.

Kinnunen, A., Tikanmäki, M., Heinonen, J., 2016. An energy model for ice crushing in ice-structure impact. In: 23 rd IAHR International Symposium on Ice, Ann Arbor, Michigan, USA, pp. 1–8.

Kjerstad, Ø.K., Metrikin, I., Løset, S., Skjetne, R., 2015. Experimental and phenomenological investigation of dynamic positioning in managed ice. Cold Reg. Sci. Technol. 111, 67–79.

Liu, Z., Amdahl, J., Løset, S., 2011. Plasticity based material modelling of ice and its application to ship-iceberg impacts. Cold Reg. Sci. Technol. 65 (3), 326–334.

Lu, W., Lubbad, R., Løset, S., 2015a. In-plane fracture of an ice floe: a theoretical study on the splitting failure mode. Cold Reg. Sci. Technol. 110 (0), 77–101.

Lu, W., Lubbad, R., Løset, S., 2015b. Out-of-plane failure of an ice floe: radial-crack-initiation-controlled fracture. Cold Reg. Sci. Technol. 119, 183–203.

Lu, W., Lubbad, R., Løset, S., 2015c. Tentative fracture mechanisms of the parallel channel effect during ice management. In: Kim, E., Lu, W., Høyland, K. (Eds.), The 23rd International Conference on Port and Ocean Engineering under Arctic Conditions, Trondheim, Norway.

Lu, W., Lubbad, R., Løset, S., Kashafutdinov, M., 2016. Fracture of an ice floe: local out-of-plane flexural failures versus global in-plane splitting failure. Cold Reg. Sci. Technol. 123, 1–13.

Lu, W., Lubbad, R., Løset, S., Skjetne, R., 2016a. parallel channel tests during ice management operations in the Arctic Ocean. In: Arctic Technology Conference 2016, St. John's, Newfoundland and Labrador.

Lu, W., Zhang, Q., Lubbad, R., Løset, S., Skjetne, R., 2016b. A shipborne measurement system to acquire sea ice thickness and concentration at engineering scale. In: Arctic Technology Conference 2016, St. John's, Newfoundland and Labrador.

Lubbad, R., Løset, S., 2011. A numerical model for real-time simulation of ship-ice interaction. Cold Reg. Sci. Technol. 65 (2), 111–127.

Lubbad, R., Løset, S., Hedman, U., Holub, C., Matskevitch, D., 2016. Oden arctic Technology research cruise 2015. In: Proc. Of the Arctic Technology Conference (ATC), St. Johns's, Newfoundland and Labardor, Canada.

Nevel, D.E., 1958. The Theory of a Narrow Infinite Wedge on an Elastic Foundation. U. S. Army Snow Ice and Permafrost Research Establishment, Corps of Engineering.

Nevel, D.E., 1965. A Semi-infinite Plate on an Elastic Foundation. U. S. Army Snow Ice and Permafrost Research Establishment, Corps of Engineering.

Nevel, D.E., 1972. The ultimate failure of a floating ice sheet. In: International Association for Hydraulic Research, Ice Symposium, pp. 17–22.

Panfilov, D., 1960. Experimental Investigation of the Carrying Capacity of a Floating Ice Plate, vol. 64. Izvestia Vsesojuznogo Nauchno-Issledovatelsskogo Instituta Gidratekhniki, pp. 80–88.

Schulson, E.M., Duval, P., 2009. Creep and Fracture of Ice, vol. 1. Cambridge University Press, Cambridge, pp. 190–211.